Investigation of chromate and nitrate removal by adsorption at the surface of an amine-modified cocoa shell adsorbent

Patrick Nkuigue Fotsing, Nabil Bouazizi, Emmanuel Djoufac Woumfo, Nadine Mofaddel, Franck Le Derf, Julien Vieillard

Investigation of chromate and nitrate removal by adsorption at the surface of an amine-modified cocoa shell adsorbent

Patrick Nkuigue Fotsing[a], Nabil Bouazizi[b], Emmanuel Djoufac Woumfo[a], Nadine Mofaddel[b], Franck Le Derf[b], Julien Vieillard[b*]

[a] Laboratory of Applied Inorganic Chemistry, Faculty of Sciences, University of Yaoundé I, PO Box 812, Yaoundé, Cameroon

[b] Normandie Univ., UNIROUEN, INSA Rouen, CNRS, COBRA (UMR 6014), 27000 Evreux, FRANCE

* Corresponding author : julien Vieillard, UMR CNRS 6014 COBRA, 55 rue Saint Germain, 27000 Evreux, France ; Email : julien.vieillard@univ-rouen.fr

Keywords: 3-aminopropyltriethoxysilane; cocoa shell; amine modified, physisorption; chemisorption; heavy metals, nitrate, adsorption

ABSTRACT

Nitrate (NO_3^-) and chromium (Cr(VI)) ions from contaminated aqueous solutions were successfully adsorbed onto functionalized cocoa shell (ECAB, an agricultural waste material) *via* chemical grafting of 3-aminopropyltriethoxysilane (APTES). The resulting adsorbent – ECAB-APTES-HCl – was characterized by SEM, zeta potential, calorimetry, FTIR spectroscopy and point of zero charge. The adsorption parameters were investigated to optimize the removal of chromium and nitrate ions. The maximum removal efficiency stabilized at around 91-99% for chromium and 58% for nitrate, for an initial concentration of 50 $mg.L^{-1}$ of the ions. The adsorption process fitted well with both Freundlich and Langmuir isotherms, and with the pseudo-second order model. Accordingly, adsorption onto ECAB-APTES-HCl involved both physisorption and chemisorption. Desorption studies demonstrated that 82% of nitrate and 79.8% of chromium were recovered in less than 2 hours. These results open onto the possible removal of

heavy metals from aqueous solutions in the absence of energy constraints, using low-cost biomass relevantly functionalized for high adsorption efficiency.

1. Introduction

Nitrate (NO_3^-) and heavy metals such as chromium [Cr(VI)] are more and more utilized with the continuous progress of industrialization. The water contaminants produced by industrial manufacturing can not only directly damage the water ecosystem but also greatly threaten human health because they are usually toxic, persistent, non-biodegradable, and accumulate in the food chain [1-4].

The environmental hazards associated with these effluents are toxicity, bioaccumulation, and effects on human health like skin irritation, dermatitis, conjunctivitis and painful colic if absorbed orally [5-8]. In view of these environmental concerns and health issues, scientists have to develop approaches and efficient adsorbents to remove heavy metal pollutants from wastewaters before discharging them into natural water bodies. Numerous methods are available for nitrate and heavy metal remediation from water, e.g., reverse osmosis, electrochemical methods, filtration, ion exchange, flocculation, or coagulation [9-11]. Adsorption is one such method. It has several advantages when compared to other methods such as ease of operation, improved efficiency, limited cost, and reusability that reduces sludge disposal issues [12, 13].

Many adsorbents have already been evaluated, but, except for biomass and derivatives, most materials have showed low adsorption capacities towards pollutants in aqueous solution [14-16]. Intensive research is being focused on promoting ecofriendly and low-cost agricultural waste materials for water treatment. Biomass is widely available in nature, and growing interest is now focused on its use as a promising source for the production of activated carbon and as a potential

alternative for adsorbing hazardous pollutants in aqueous solution [17-19]. However, biomass materials remain a major issue as to surface functionalization and activation, and several studies have already been carried out to overcome these shortcomings. The relatively limited number of functional groups at the biomass surface seriously impedes the efficient use of numerous adsorbents for practical applications in the removal of toxic molecules from water.

A relevant approach consists in functionalizing non-polluting biomass through impregnation with polymers and amines. Adsorbent-pollutant interactions are an essential requirement in this respect, and can be achieved using basic chemical functions of materials such as hydroxyl and amine groups. Amine-enriched materials have already showed high affinity towards toxic pollutants in water [20-22]. The improvement of their affinity was explained in terms of mere incorporation of a vegetal source of -OH and -NH_2 groups. Unlike composite materials (zeolites, metal-organic frameworks (MOFs), and others) tested in the removal of chromate and nitrate ions, low-cost natural materials such as vegetal waste display low surface acidity and do not require sophisticated modification procedures. The structure of all vegetal materials bears terminal hydroxyl and amine groups but does not necessarily exhibit interesting affinity towards organic and inorganic pollutants due to structure constraints. This is why vegetal waste modification often turns out to be an essential requirement to improve affinity for pollutants.

Nitrate and heavy metal binding is required to use amine derivate to remove heavy metals from water by adsorption. Structural groups like -COOH, -NH and -OH present in natural and modified polymer (cellulose, chitosan, lignin) act as active sites for nitrate and heavy metal binding by hydrogen bonding, hydrophobic interactions or complexation [23, 24].

The present study is focused on cocoa shell (ECAB), a byproduct of the cocoa industry. ECAB was chemically modified by 3-aminopropyltriethoxysilane grafting through silanization, followed by a protonation step. Such a chemical modification is supposed to improve the

adsorption properties of ECAB. Nevertheless, the role of amine in nitrate and chromium adsorption onto a solid surface remains to be elucidated, more particularly on OH- and/or NH_2-enriched solid surfaces, where competitive interactions can occur between pollutants and adsorbent surfaces bearing -NH_2 and/or -OH and -COO^- groups. The originality of this approach lies in (i) the attempts to induce both physical and chemical interactions to capture pollutants, and (ii) a comparative study with our similar recently published work. For this purpose, the comparison with our previous work was correlated with the surface properties and adsorption performances [21, 25]. A comprehensive characterization through physicochemical techniques such as FTIR and DSC spectroscopy, scanning electron microscopy and zeta potential provided valuable insights. Moreover, the behavior of the adsorbents towards pollutants was examined in terms of equilibrium isotherms and kinetic studies.

2. Materials and methods

2.1. Chemicals

Potassium dichromate ($K_2Cr_2O_7$, 99%), sulfuric acid (95%), absolute ethanol (EtOH, 99%), 1.5-diphenylcarbazide ($C_{13}H_{14}N_4O$, 98%), 3-aminopropyltriethoxysilane (APTES, 98%), hydrochloric acid (37%), acetic acid (CH_3COOH, 96%), sodium hydroxide (98%), ethylenediaminetetraacetic acid disodium salt ($C_{10}H_{14}N_2Na_2O_8$, $2H_2O$, 99%), sodium nitrate ($NaNO_3$, 99%), potassium nitrate (KNO_3, 99%), salicylic acid ($C_7H_5NaO_3$, 99%), sodium phosphate monobasic monohydrate (H_4NaO_5P), and sodium azide (NaN_3, 99.5%) were purchased from Merck (France) and used as supplied. All the solutions were prepared using double distilled water (Merck, Millipore).

2.2. Preparation and functionalization of modified cocoa shell

The functional ECAB-APTES-HCl and ECAB materials were prepared as follows:

i) Firstly, cocoa shell was collected from a local farm managed by the IRAD (Institute of Agricultural Research for Development) at Yaoundé, Cameroon. It was cut, washed with acidic water (HCl, 1 mol.L^{-1}) to remove organic matter, sun-dried for 5 days and then heated at 70 °C overnight to remove moisture. Then it was ground and sifted at 160 µm. The resulting powder was named ECAB.

ii) Secondly, APTES was chemically grafted using water/ethanol 1:3 (V/V) as a solvent, and a mixture of ECAB/APTES 1:3 (W/W) at 80 °C for 5 hours. The synthesized product, named ECAB-APTES, was filtered (0.45 µm filter paper under vacuum (Fisherbrand)), washed several times, and then dried at 70 °C overnight [26].

iii) Finally, ECAB-APTES was acidified using HCl solution to protonate the amino groups and lead to positively charged ammonium moieties [27]: 1 g of ECAB-APTES was stirred in 100 mL of 0.5 mol.L^{-1} HCl for 2 h at room temperature. The acidified material, named ECAB-APTES-HCl, was recovered by filtration, washed several times, and then dried at 70 °C overnight (**scheme 1**).

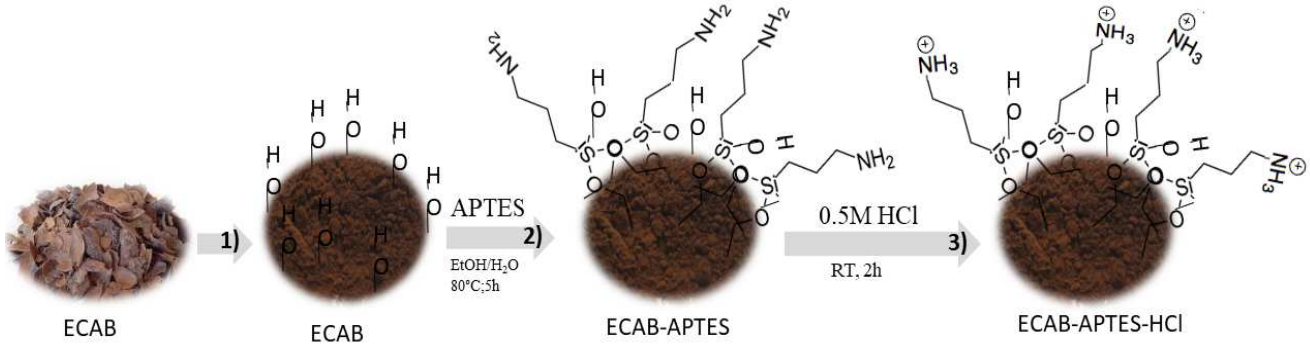

Scheme 1: Schematic illustration of the ECAB-APTES-HCl preparation procedure: 1) preparation of ECAB agricultural waste; 2) chemical grafting of APTES; 3) protonation step.

2.3. Characterization of the material

ECAB, ECAB-APTES and ECAB-APTES-HCl were characterized by scanning electron microscopy (SEM), EDS (energy dispersive X-ray spectroscopy), Fourier transforms infrared spectroscopy (FTIR), and differential scanning calorimetry (DSC); moreover, the points of zero charge (pH_{pzc}) were determined. For SEM, adsorbents were metallized by a gold layer at 18 mA for 360 s using a Biorad E5200 device. Then, SEM images were acquired using a ZEISS EVO 15 electron microscope. Two types of images were recorded: secondary ion images to observe the morphology of the surface, and EDS images to evaluate the chemical contrast. FTIR analysis was performed using a Tensor 27 (Bruker) spectrometer with a ZnSe ATR crystal in the 4000 – 500 cm^{-1} wavenumber range. For each spectrum, 20 scans were recorded with a resolution of 4 cm^{-1}. DSC of the samples was carried out with a DSC – 131 Setaram, with a 20 °C to 500 °C temperature range and a heating rate of 10 °C.min^{-1}. The zeta potential was measured for each sample dispersion using the phase analysis light scattering (PALS) mode and a Malvern zeta sizer nano ZS setup.

The pH values at the point of zero charge (pH_{pzc}) of ECAB, ECAB-APTES and ECAB-APTES-HCl were determined by the solid addition method [28], using a Consort C 863 electronic multiparameter analyzer. The initial pH value (pH_i) of 50 mL of 0.1 mol.L^{-1} of $NaNO_3$ solution was roughly adjusted in the 2 -12 pH range using 0.1 mol.L^{-1} NaOH and HCl. Then, 0.1 g of each sample was placed in a 100-mL conical flask for 48 h to reach equilibrium at ambient temperature. After that, the final pH (pH_f) of the solutions was measured, and pH_{pzc} was determined as $\Delta pH = 0$ from a plot of ($pH_f - pH_i$) *versus* pH_i.

2.4. Adsorption study

Batch adsorption experiments were carried out at 300 rpm and at room temperature in 100-mL shaking flasks containing 0.2 g of adsorbent and 50 mL of ions at different concentrations (from 50 to 400 mg.L^{-1}). The effects of different parameters (contact time, pH, initial concentration),

were also examined. Adsorption kinetics were obtained at T = 20 °C and pH_i = 5.5 and 4.5 for nitrate and Cr(VI), respectively. After shaking for an appropriate time, ECAB and modified ECAB samples were separated from the solution using 0.45 µm filter paper under vacuum (Fisherbrand). Then, the solutions were analyzed by colorimetry with the 1,5-diphenylcarbazide method (λ = 540 nm) for Cr(VI) [29] and with the sodium salicylate method (λ = 415 nm) for NO_3^- [30], using a UV-visible spectrophotometer (SHIMADZU UV-1640). The influence of competitive PO_4^{3-} ions was also evaluated. A mixture of 50 mg.L^{-1} of Cr(VI) and 50 mg.L^{-1} of PO_4^{3-} ions was prepared and incubated with ECAB-APTES-HCl for 300 minutes. Then, 10 mL of the mixture were filtered (0.45 µm filter paper under vacuum (Fisherbrand), mixed with ammonium molybdate (1 mL) and hydrazine sulfate (0.4 mL) heated at 60 °C for 30 min. Then, the absorbance of the ammonium phosphomolybdate complex was measured at 830 nm.

The amounts of adsorbed Cr(VI) or NO_3^- (q_e in mg/g) at equilibrium were calculated using equation (1),

$$q_e = \frac{(C_0 - C_e) \times V}{m} \quad \textbf{(1)}$$

where C_o and C_e are the initial and equilibrium concentrations of Cr(VI) (mg.L^{-1}), respectively, V is the volume of solution (L) and m is the mass of adsorbent used (g).

The adsorption yield was estimated using equation (2):

$$E\ (\%) = \frac{(C_0 - C_e)}{C_0} \times 100 \quad \textbf{(2)}$$

2.5. Desorption experiments

Batch desorption experiments were conducted by stirring a solution of the adsorbent and 0.1 mol.L^{-1} NaOH for 180 minutes. When NaOH was used as an eluting agent, the interactions

between ECAB-APTES-HCl and Cr/nitrate were disrupted, and chromate/nitrate ions were released into the eluent. Therefore, NaOH was selected to better compare and understand the results with previously published ones [25]. Then, the solutions were filtered under vacuum and analyzed by the 1,5-diphenylcarbazide method for Cr(VI) and the sodium salicylate method for NO_3^- using a UV-Vis spectrophotometer. The amount of desorbed Cr(VI) et NO_3^- ions (q_{des} in $mg.g^{-1}$) were calculated using equation (3) [31]

$$q_{des} = \frac{C_{des.} \times V}{m} \quad (3)$$

where C_{des} is the delivered concentration of Cr(VI) or NO_3^- ($mg.L^{-1}$), V is the volume of solution (L) and m is the mass of adsorbent (g). Then, desorption yields were estimated using equation (4).

$$Percent\ of\ desorption = \frac{amount\ of\ desorbed\ NO_3^-\ or\ Cr(VI)}{amount\ of\ adsorbed\ NO_3^-\ or\ Cr(VI)} \times 100 \quad (4)$$

3. Results and discussion

3.1. Characterization

The surface morphologies of ECAB and ECAB-APTES-HCl were analyzed by SEM microscopy (**Figure 1a**). The surfaces of the untreated cocoa shell and modified cocoa shell were obviously different. ECAB exhibited a smoother surface than modified ECAB. ECAB also presented particle agglomerates coming from pectin, cellulose, lignin and wax, which were less visible after APTES modification [32]. Foils corresponding to silane grafting were observed only on the ECAB-APTES-HCl surface. HCl post-treatment caused holes to appear on the APTES foils (**Figure S1**). This trend can be explained by the strong interaction between amino groups and acidic protons.

To confirm the successful chemical grafting of APTES, the samples were analyzed by EDS (**Figure 1**). The Au, Cu and Pd heteroatoms in the EDS spectra came from the metallization process. After APTES modification, the peaks corresponding to carbon, oxygen and silicon were more intense, confirming the presence of organosilane grafting. The peak at 2.6 keV was assigned to chlorine from HCl treatment.

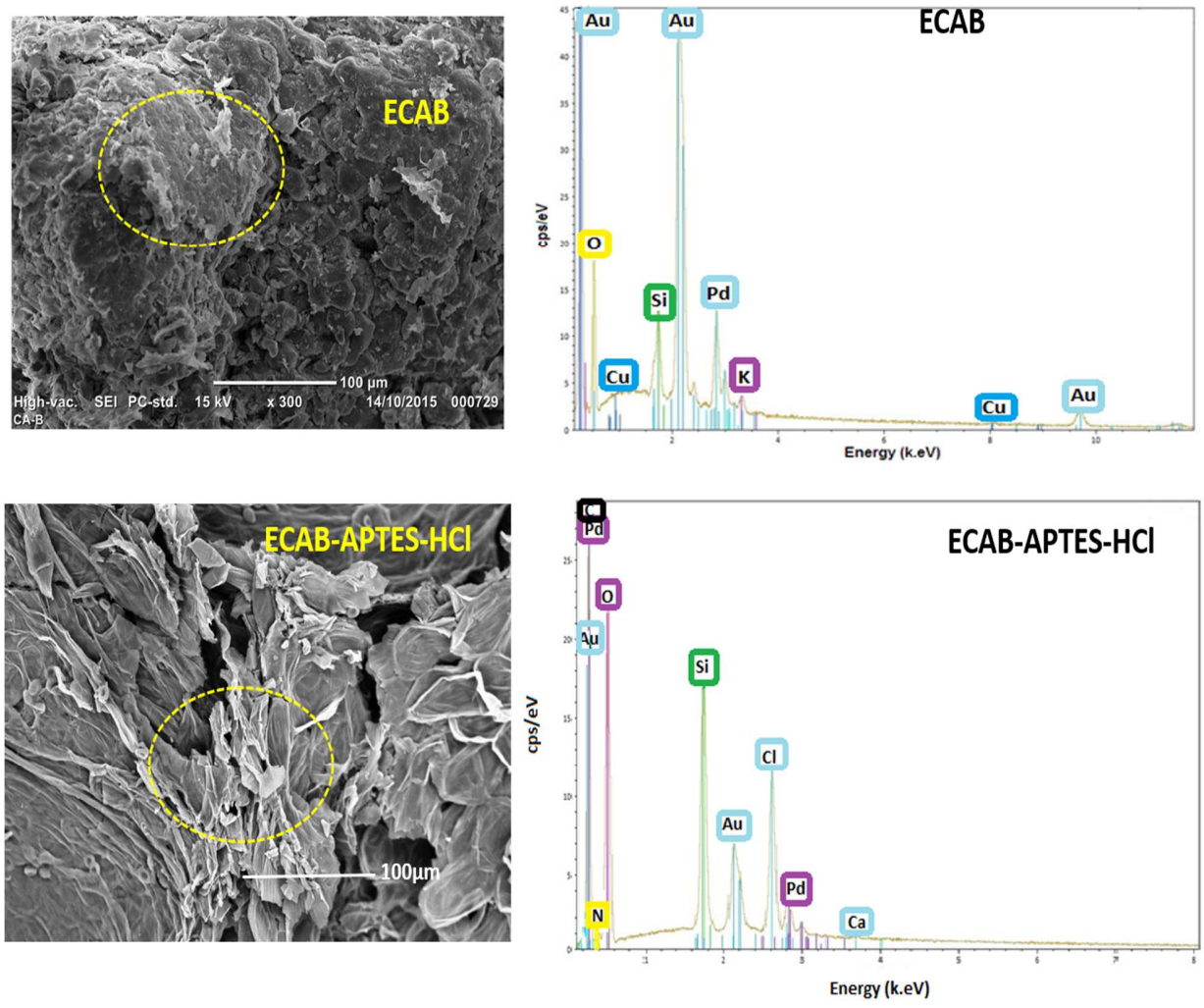

Figure 1: SEM images, with elemental composition and morphology of the ECAB and ECAB-APTES-HCl adsorbents.

The ECAB adsorbent and its modified counterpart were characterized by FTIR analysis (**Figure S2b**). The spectra of the APTES molecules is reported separately in **Figure S2a** to facilitate comparisons and interpretations. The absorption bands of hydrolyzed APTES were described by different vibrational modes related to NH_2, CH_2, and Si-O bonds. The peaks observed at 3300 cm^{-1} and 3290 cm^{-1} were associated to the asymmetric and symmetric stretching modes of NH_2, respectively [33]. However, the band was related to the Si-OH groups at 3200 cm^{-1}, whereas the stretching modes of CH_2 were observed at 2932 cm^{-1} and 2883 cm^{-1}. In addition, the amine function (NH_2) was observed at 1562 cm^{-1} and 1484 cm^{-1}. The Si-O-Si bond was observed at 1130 cm^{-1} and 1044 cm^{-1} [33]. Regarding the initial adsorbent (ECAB), FTIR spectra displayed distinguishable peak patterns in agreement with the literature [34]. The FTIR spectra of ECAB presented a characteristic strong band at around 3350 cm^{-1} associated with the stretching vibration of the hydroxyl groups from cellulose, hemicellulose and lignin. Some bands at 2923 and

2881 cm^{-1} corresponding to the stretching vibration of the $–CH_2$ groups were also present. The band at around 1000 cm^{-1} was associated to the oxygen functional groups C-O [35]. After APTES grafting, the intensity of these bands was lower due to the formation of C–O–Si– bonds. New bands at 1062 and 916 cm^{-1} associated to the stretching vibration of Si–O–Si and Si–O–C, respectively, confirmed this hypothesis [36]. Small bands at 709 and 644 cm^{-1} assigned to the stretching vibration of Si–C came from the propylsilane function. After acidic treatment, the increase of the IR peak at 3336 cm^{-1} was associated to the stretching vibration of NH_3^+, whereas peaks at 1720 and 1514 cm^{-1} were assigned to the symmetric and antisymmetric stretching vibration of N–H, respectively [37, 38]. Furthermore, new bands at 676 and 1180 cm^{-1} attributed to the stretching vibration of Si–C and C–N, respectively, confirmed the chemical grafting of APTES and its protonation [38, 39]. Some visible changes on the FTIR spectra were observed

after the adsorption of chromate and nitrate (**Figure S2c**). The intensity of the peak at 1180 cm^{-1} corresponding to the C–N band was lower and even absent after Cr(VI) adsorption, confirming that the amino group was involved in the binding of anions. After nitrate adsorption, the peak at 3336 cm^{-1} shifted to a higher wavenumber, indicating that NH_3^+ was involved in the interaction. Nitrate adsorption was also confirmed by the increase of the signal at 1400 cm^{-1}, which is characteristic of the NO_3 asymmetric stretching vibration.

DSC analysis in the 25 - 500 °C temperature range was also performed to investigate the thermal stability of modified ECAB (**Figure 2a**). The endothermic peaks observed at around 126 °C were attributed to the dehydration of the samples. From 200 to 250 °C, an exothermic peak corresponded to the degradation of cellulose, lignin and hemicellulose [26, 40]. In the 350 - 400 °C range, the two exothermic peaks at 363 and 392 °C corresponded to silane degradation. Thus, APTES and APTES-HCl treatment increased the thermal stability of ECAB in the 250 - 400 °C range. All these results are in agreement with the literature and with SEM and IR data.

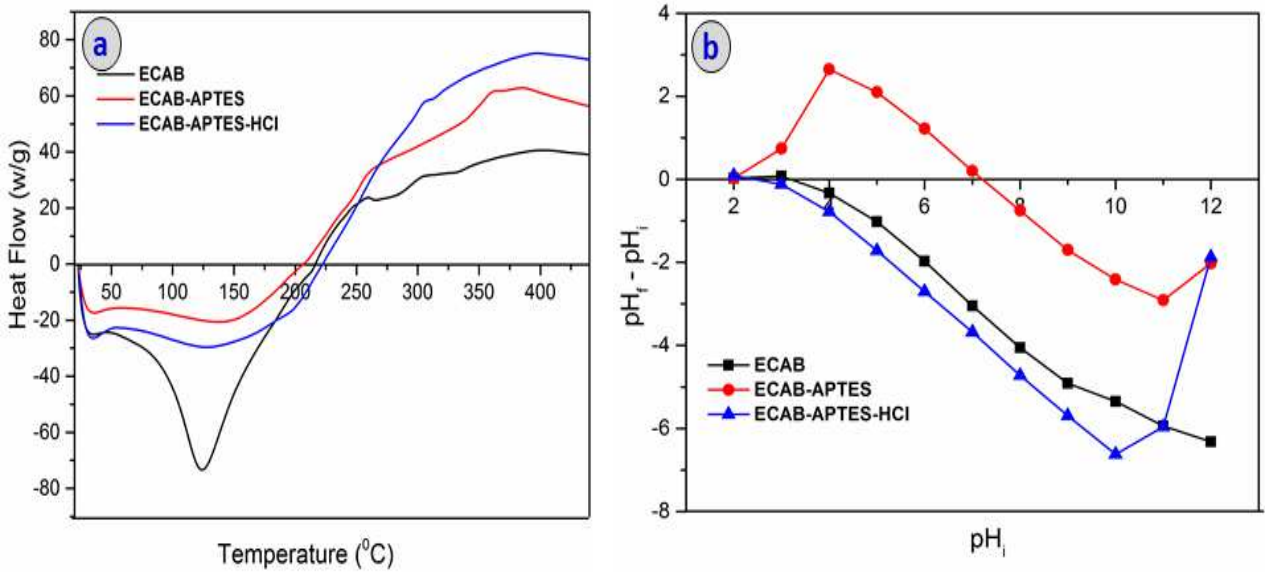

Figure 2: DSC (a) and point of zero charge profiles (b) of ECAB, ECAB-APTES and ECAB-APTES-HCl.

To determine the surface acidity of all adsorbents, their points of zero charge were measured (**Figure 2b**). pH_{pzc} were found at pH values of around 3.4 for ECAB and 7.2 for ECAB-APTES. When comparing the pH_{pzc} values of different adsorbents, it was clear that the lowest pH_{pzc} was recorded for the initial material (ECAB), lower than that of other agricultural waste materials such as olive stone (4.2) and sugar cane bagasse (5.7) [41].

ECAB was altogether negatively charged over a wide range of pH values, suggesting the presence of functional groups (COO^-, OH^-) on its cellulose and lignin moieties. pH_{pzc} analyses of ECAB-NH_2 indicated that APTES treatment affected the deprotonation of the cellulosic structure with a positive surface charge over a wider pH range (2.0 - 7.2) than ECAB [42]. Therefore, pH_{pzc} measurements confirmed the successful grafting of amino groups onto the ECAB surface. These results are in agreement with those obtained by DSC, SEM and FTIR analyses. After acidic activation, pH_{pzc} decreased from 7.2 for ECAB-APTES to 2.8 for ECAB-APTES-HCl, indicating a lower surface charge. In addition, the zeta potential recorded at pH 7 shifted from -20 mV for ECAB to 0 mV for ECAB-APTES-HCl, suggesting high stability of the adsorbent. Importantly, zeta potential (ZP) measurements performed after Cr(VI) and nitrate adsorption indicated a negative ZP (-4 mV). This negative value confirmed that anions were adsorbed onto ECAB-APTES-HCl. Consequently, functionalized ECAB could be a good candidate for Cr(VI) and nitrate capture *via* electrostatic interactions.

3.2. Adsorption study

3.2.1. Parameter effects

Figure 3 describes the amounts of Cr(VI) and NO_3^- adsorbed by different adsorbents as a function of the contact time. The adsorption process was dependent on the initial amounts of anions: the higher the initial anion concentration, the more anions were adsorbed. We evaluated the adsorption yields of ECAB and ECAB-APTES as controls. The adsorption capacity of the raw material ECAB was 0.94 $mg.g^{-1}$ for Cr(VI) and 1.04 $mg.g^{-1}$ for NO_3^- at an initial concentration of 50 $mg.L^{-1}$. The weak adsorption yield recorded for ECAB can be explained by the presence of substantial numbers of hydroxyl groups at its surface, which caused electrostatic repulsion preventing the capture of pollutants. This result was confirmed by the ZP measurements, where ECAB displayed negative values (-20 mV) due to the hydroxyl groups that decreased the adsorption process. The adsorption capacities of ECAB-APTES were ~ 0 $mg.g^{-1}$ for Cr(VI) and 1.87 $mg.g^{-1}$ for NO_3^-. For the same initial concentration of Cr(VI) and NO_3^-, the adsorption capacity of ECAB-APTES-HCl was 7 $mg.g^{-1}$ for Cr(VI) and 12 $mg.g^{-1}$ for NO_3^-. The profile of the adsorption curve of ECAB-APTES-HCl could be explained by a large amount of active sites on the surface that were not totally in interaction with ions at low concentrations. The adsorption rate proceeded in two steps, with a fast adsorption process from 0 to 60 minutes and a lower rate later. First, all the adsorption sites of the adsorbent surface were available, and the mass transfer of anions from the solution to the adsorbent was facilitated [40, 43, 44]. Then, the adsorption rate decreased, and was lower in the presence of higher anion concentrations because diffusion into the boundary film layer at the surface and into the structure was slower. The equilibrium state was reached at t = 180 minutes for NO_3^- and t = 240 minutes for Cr(VI).

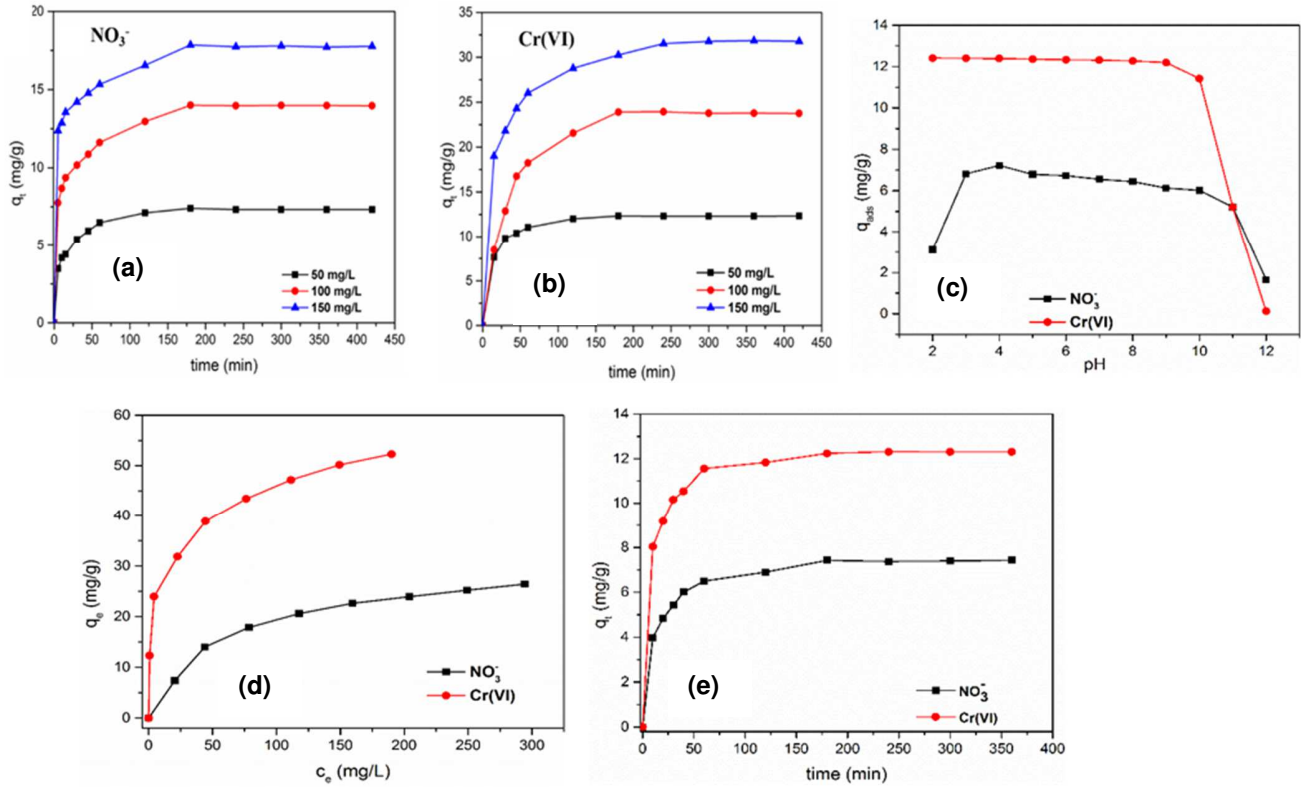

Figure 3: Effect of (a-b) the contact time, (c) the pH, (d) the initial concentrations, and (e) PO_4^{3-} on NO_3^- and Cr(VI) adsorption onto ECAB-APTES-HCl (m = 0.2 g; 300 rpm; pH_i = 5.6 for nitrate and 4.6 for chromate; V = 50 mL).

The role of pH_i on Cr(VI) and NO_3^- adsorption was examined (**Figure 3c**). It revealed a pH-independent adsorption process within a large range of pH values. The maximum removal efficiency indeed stabilized at around 91 - 99% for chromium ions between pH 2 and pH 10. To clarify the mechanisms involved in these interactions, the diagram of Cr speciation in the pH range is presented in **Figure S3**. At higher pH values, the adsorption capacity plummeted from 91% to 0.9%. Such a drop may result from a lower transfer of protons from the surface to the solution resulting in a negatively charged surface [29, 37, 43]. This drop may also come from the high amount of hydroxide ions, which competed with hydrogen chromate [37, 40, 45]. As for NO_3^-, maximum removal efficiency reached 57.8% at pH 4. In the 5 to 11 pH range, the

adsorption yield was close to the maximum value, indicating that the process was mainly pH-independent. Similarly to Cr(VI) ions, NO_3^- ions were sensitive to high pH values due to the large amount of hydroxide anions in competition in this context [28, 46]. So, in this work, the adsorption mechanism of ECAB-APTES-HCl seemed to be sensitive to electrostatic interactions.

The amount of phosphate ions is limited in natural water bodies. However, phosphate ions can be found in domestic or industrial water, so they were used to evaluate the effect of coexisting ions on NO_3^- or chromate adsorption onto ECAB-APTES-HCl (**Figure 3e**). Contaminated solutions were prepared with equal concentrations of NO_3^-, phosphate or Cr(VI) ions to carry out a competitive assay. The NO_3^- and Cr(VI) adsorption yields were not influenced by the presence of phosphate ions. These results confirm that the adsorption process onto ECAB-APTES-HCl is controlled by electrostatic interactions but also by the structural organization of the ECAB-APTES-HCl surface. For nitrate, the negative charge is delocalized between the 3 oxygens, and this facilitates multiple electrostatic interactions with different positive charges distributed across the surface of ECAB-APTES-HCl [47].

3.2.2. Adsorption kinetics

The kinetics of heavy metal and organic pollutant adsorption onto solid adsorbents are usually investigated using pseudo-first order and pseudo-second order kinetic models. Our experimental data were simulated by applying the pseudo-first order (Eq. (5)), pseudo-second order (Eq. (6)), Elovich (Eq. (7)), and intra-particle diffusion (Eq. (8)) equations.

$$\log(q_e - q_t) = \log q_e - k_1 \frac{t}{2.303} \quad \textbf{(5)}$$

$$\frac{t}{q_t} = \frac{1}{k_2 q_e^2} + \frac{t}{q_e} \quad \textbf{(6)}$$

$$q_t = \frac{1}{\beta}\ln(\alpha\beta) + \frac{1}{\beta}\ln(t) \quad \textbf{(7)}$$

$$q_t = k_{id}\, t^{1/2} + C_i \quad \textbf{(8)}$$

where q_e and q_t ($mg.g^{-1}$) are the amounts of the adsorbate adsorbed *per* unit weight of adsorbent at equilibrium time and time t (min), respectively; k_1 (min^{-1}), k_2 ($g.mg^{-1}.min^{-1}$), and k_{id} ($g.mg^{-1}.min^{-0.5}$) are the pseudo-first order rate constant, pseudo-second order equilibrium rate constant, and intra-particle diffusion rate constant, respectively; as regards Elovich coefficients, α is the initial adsorption rate ($mg\ g^{-1}.min^{-1}$) and β is the desorption constant ($g.mg^{-1}$) during any one experiment; C_i is the intercept related to the thickness of the boundary layer.

The pseudo-first order kinetic model generally suggested that adsorption occurred through physisorption, whereas the pseudo-second order indicated that adsorption occurred through chemisorption [48]. **Figure 4** and **Table 1** show that most of nitrate and heavy metal are adsorbed onto functionalized ECAB. These datas fitted well with the pseudo-second order kinetic model, as supported by the correlation coefficients. Therefore, for instance the ECAB adsorbent involved chemisorption, as well as physisorption as estimated by the pseudo-first order model.

In this respect, other researchers created an intraparticle diffusion kinetic model that determines the adsorption process of adsorbates [49, 50]. Mohan et al. assumed that intraparticle diffusion was the best model describing the mass transfer of adsorbates [51]. Experimental data closely fitted with this model (R^2=0.98), indicating that the intra-particle diffusion model could be satisfactorily applied in 2 steps. The first step can be attributed to the diffusion of the ions through the solution to the external surface of the adsorbent. The second step, describes the final equilibrium where the intra-particle diffusion is limited. Thus, at the beginning, the rate of the adsorption is controlled by intra-particle diffusion and then it was mostly due to chemisorption.

330 Regarding the intraparticle diffusion curves, a visible change in the slope was observed,
331 beginning at t = ~ 10 min. The results evidenced the existence of two adsorption types (i.e.,
332 physical and chemical). Afterward, physisorption was probably involved during the adsorption of
333 pollutants onto functionalized ECAB. In addition, a previously published work also reported
334 adsorption through physisorption [52]. Physisorption is an easily reversible phenomenon, which
335 improves the regeneration process. ECAB-APTES-HCl allowed for substantial regeneration of
336 both pollutants (*will be discussed in the following section*), suggesting the presence of weak
337 physisorption. Consequently, NO_3^- and Cr adsorption occurred via physisorption and
338 chemisorption.

339

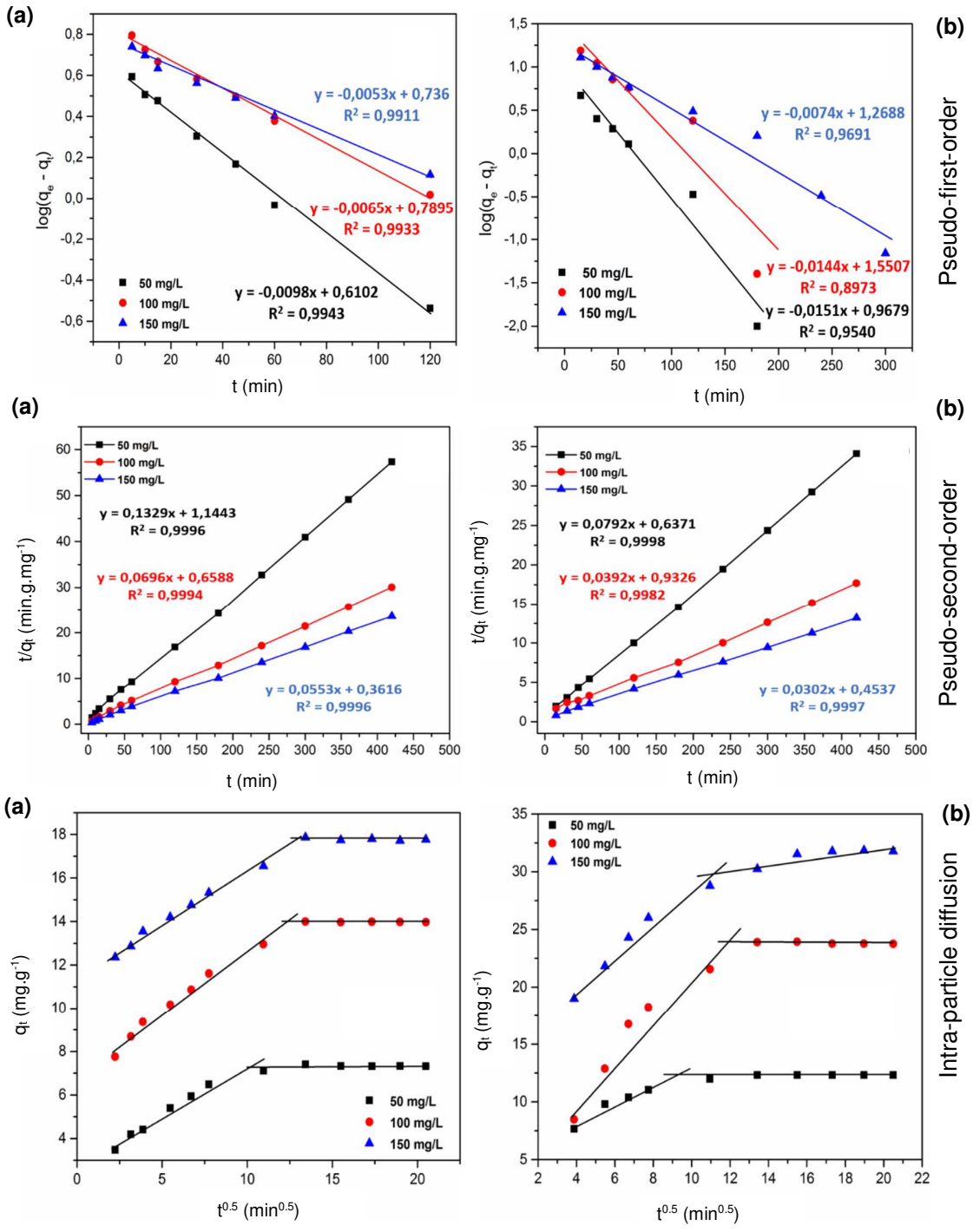

Figure 4: Pseudo-first order, pseudo-second order kinetics and intra-particle diffusion model of nitrate (a) and Cr (VI) (b) removal by ECAB-APTES-HCl.

359 **Table 1:** Summary of the kinetic parameters (k, R^2, q_e) of NO_3^- and Cr(VI) adsorption onto
360 ECAB-APTES-HCl. (m = 0.2 g, pH_i = 5.6 for nitrate and 4.6 for chromate, 300 rpm, V = 50 mL,
361 room temperature).

	Concentration of NO_3^- (mg/L)			**Concentration of Cr(VI) (mg/L)**		
Parameters/coefficients /constants	50	100	150	50	100	150
$q_{e,\,exp}$ (mg.g^{-1})	**7.41**	**14.00**	**17.86**	**12.33**	**23.94**	**31.85**
Pseudo-first order						
k_1 (min^{-1})	0.022	0.015	0.012	0.035	0.033	0.017
$q_{e,cal}$ (mg.g^{-1})	4.076	6.159	5.445	9.287	35.538	18.570
R^2	0.9943	0.9933	0.9911	0.9540	0.8973	0.9691
Pseudo-second order						
k_2 (g.mg^{-1}.min^{-1})	0.015	0.007	0.008	0.010	0.002	0.002
$q_{e,cal}$ (mg.g^{-1})	7.524	14.368	18.083	12.626	25.510	33.112
R^2	0.9996	0.9994	0.9996	0.9998	0.9982	0.9997
Elovich						
α (mg.g^{-1}.min^{-1})	9.656	44.422	900.848	79.014	3.017	35.398
β (g.mg^{-1})	1.072	0.646	0.719	0.785	0.218	0.248
R^2	0.9482	0.9772	0.9708	0.8734	0.9229	0.9749
Intra-particle diffusion						
k_{1d} (mg.g^{-1}.min$^{-1/2}$)	0.427	0.584	0.479	0.854	1.817	1.384
C_1 (mg.g^{-1})	2.841	6.850	11.485	4.642	2.952	14.360
R^2_1	0.9544	0.9796	0.9871	0.9427	0.9208	0.9574
k_{2d} (mg.g^{-1}.min$^{-1/2}$)	-0.01	-0.003	-0.012	0.027	-0.026	0.1989
C_2 (mg.g $^{-1}$)	7.510	14.030	17.99	11.837	24.274	28.026
R^2_2	0.5668	0.3181	0.3662	0.5020	0.7176	0.6802

362

363 The diffusion mechanism involved in the adsorption process was predicted more precisely by
364 calculating correlation factors. The correlation factor for nitrate showed estimated values ranging
365 from 0.95 to 0.98, indicating that the intra-particle diffusion model could be satisfactorily applied
366 for the first step of the nitrate adsorption process. Therefore, during the first 60 minutes, the
367 adsorption process was mainly controlled by intra-particle film diffusion [23, 43, 53]. For Cr(VI),
368 the adsorption process was also attributed to intra-particle diffusion during the first step, but other
369 mechanisms were also probably involved because the correlation factor ranged from 0.92 to 0.95.

The second part of the curves corresponded to the slower process, when pore diffusion is the limiting step because the main parts of the active sites are occupied [53]. The k_{1d} constants were consistently higher with Cr(VI) than with nitrate, indicating that the sorption process was more intense and faster with Cr(VI) than with nitrate. This phenomenon could be explained by the higher molecular weight of Cr(VI) anions as compared to nitrate anions [54].

In both cases, the intra-particle diffusion model was not the only rate-determining mechanism, as the q_t *versus* $t^{0.5}$ curve did not go above zero. Therefore, other mechanisms such as mass transfer from the bulk solution to the adsorption center underneath the adsorbent surface were probably involved [55]. The mass transfer factor model developed by Fulazzaky *et al.* was applied to Cr(VI) and nitrate data (**Figure S4**) [56]. The global mass transfer factors $(k_La)_g$ of both ions decreased quickly, confirming that the number of occupied active sites increased with time. The low value of the external mass transfer factor $(k_La)_f$ indicated that the process was controlled by the internal mass transfer factor $(k_La)_d$. Therefore, the adsorption rate was mainly controlled by ion diffusion to the acceptor site of the adsorbent.

3.2.3. *Adsorption isotherms*

Exploring the adequate mechanisms involving adsorption onto functionalized ECAB requires the study of adsorption isotherms. The most useful isotherms to investigate adsorption equilibrium data are Freundlich and Langmuir isotherms. The adsorption data were fitted with Freundlich (Eq 9), Langmuir (Eq 10), Temkin (Eq 11) and Dubinin-Radushkevich (Eqs 12-14) models to optimize the design of the adsorption process and remove both anions from water.

$$lnq_e = lnK_F + \frac{1}{n_F} lnC_e \quad \textbf{(9)}$$

$$\frac{C_e}{q_e} = \frac{1}{q_{max} K_L} + \frac{1}{q_{max}} C_e \quad \textbf{(10)}$$

$$q_e = BlnA + BlnC_e \quad \textbf{(11)}$$

$$lnq_e = lnq_{max} - B_D \varepsilon^2 \quad \textbf{(12)}$$

$$\varepsilon = RTln\left(1 + \frac{1}{C_e}\right) \quad \textbf{(13)}$$

$$E = \frac{1}{\sqrt{2B_D}} \quad \textbf{(14)}$$

where q_e (mg.g^{-1}) and C_e (mg.L^{-1}) are the sorbate equilibrium concentrations in the solid and liquid phases, respectively; q_{max}(mg.g^{-1}) is the monolayer capacity of the sorbent; K_L (L.mg^{-1}) is a constant of the Langmuir isotherm. K_F (L.g^{-1}) is the Freundlich constant, and 1/n is the heterogeneity factor. B and A are the Temkin constants. B_D (mol^2.kJ^{-2}) is the activity coefficient, useful to obtain the mean sorption energy E (kJ.mol^{-1}), and Ɛ is the Polanyi potential. R is the gas constant (J.mol^{-1}.K^{-1}), and T is the temperature (K).

Figure 5 shows the adsorption isotherms recorded for all adsorbates. **Table S1** presents the calculated isotherm constants and the square of the regression coefficients. The highest correlation coefficients were obtained with the Langmuir model, indicating that sorption was a chemical phenomenon that took place on a homogeneous surface through monolayer adsorption [23, 46]. Based on the Langmuir model, the maximum monolayer adsorption capacity was high and estimated to be 31.64 mg.g^{-1} for nitrate and 53.19 mg.g^{-1}for Cr(VI). The fitting of the Freundlich model also gave a good correlation coefficient, indicating that the adsorption process of the two anions was reversible. This interpretation is in accordance with the low affinity constant (K_L) obtained from Langmuir data. K_F represents the adsorption capacity of the adsorbent and n_F the adsorption intensity. The high values of the two parameters confirmed that

ECAB-APTES-HCl had a good and strong adsorption capacity [43, 57]. The positive value of the Temkin constants A and B indicated that the adsorption of nitrate and Cr(VI) was endothermic and mainly occurred through physisorption [58, 59]. The Dubinin-Radushkevich (D-R) model was used to estimate the apparent free energy of adsorption and the type of adsorption. Based on the low value of the mean sorption energy E for nitrate and Cr(VI), D-R calculations confirmed that biosorption was mainly physisorption. These results altogether confirmed again the occurrence of both physisorption and chemisorption [60].

By comparing the results obtained in this work with those from numerous adsorbents reported in the literature for removal of nitrate and Cr(VI), ECAB-APTES-HCl adsorbed more nitrate than biochar or modified activated carbon did, indicating that this simple strategy of modification is an efficient way to capture nitrate **(Table 2)**.

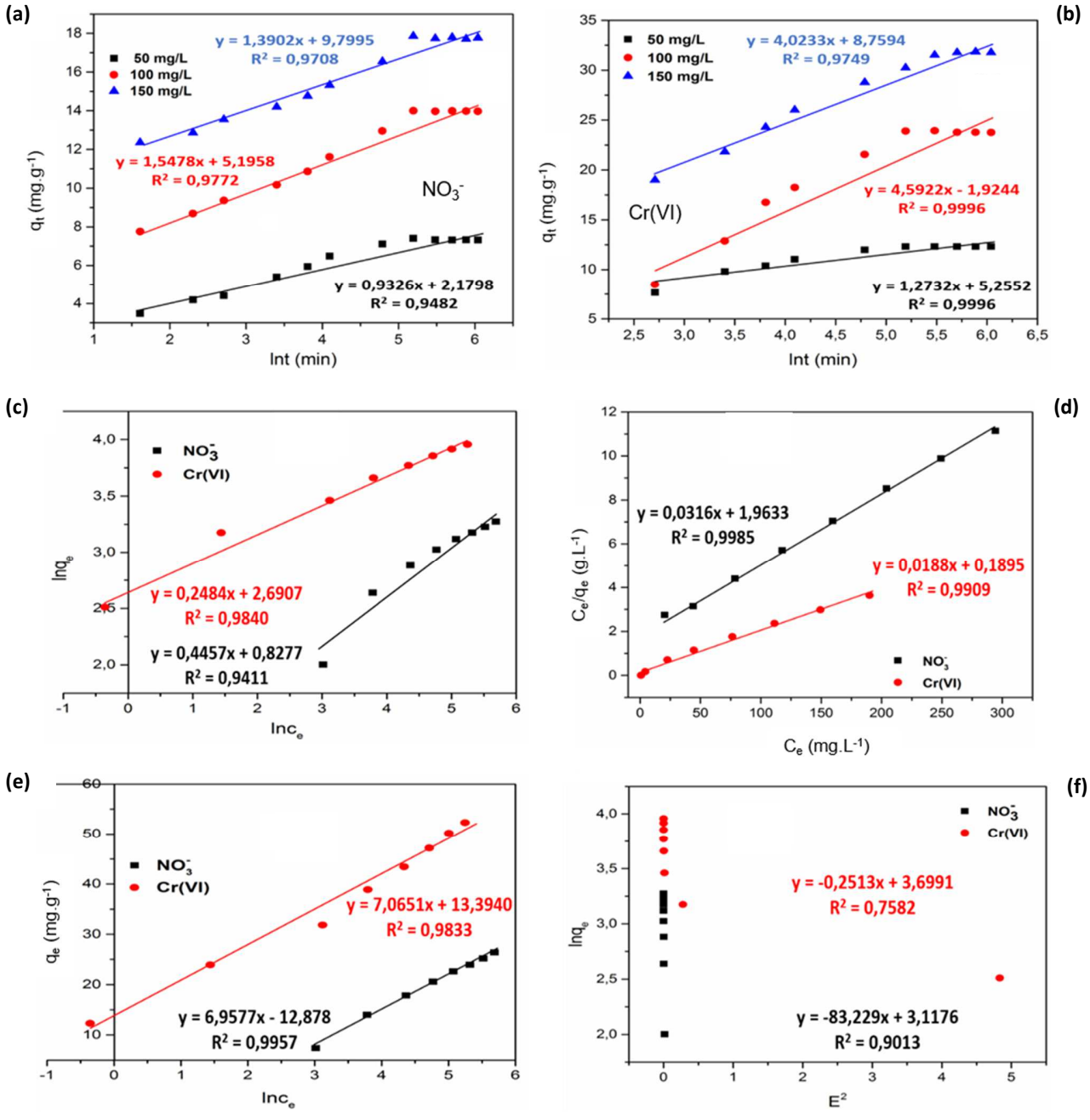

Figure 5. Elovich model (a-b) and equilibrium adsorption isotherms: (c) Freundlich, (d) Langmuir, (e) Temkin, and (f) Dubinin-Radushkevich models for NO_3^- and Cr(VI) adsorption onto ECAB-APTES-HCl (m = 0.2 g, pH_i = 5.6 for nitrate and 4.6 for chromate, 300 rpm, V = 50 mL, room temperature).

Table 2: Comparison of the results obtained in this work with other recently published studies

Biosorbent name	Functionalization	Capacity (mg/g)	Reference
NO_3^-			
Modified granular activated carbon	[3-(methacryloylamino)propyl]-trimethylammonium chloride	26	[46]
Cellulose	epichlorohydrin	218.23 (293 K)	[5]
Giant reed	triethylamine	118.9	[61]
Corn stalks	ethylenediamine	65.36 (298 K)	[62]
Sugarcane bagasse biochar	ethylenediamine	28.21	[28]
PEG/chitosan and PVA/chitosan	polyethylene glycol and polyvinyl alcohol	50.68-35.03	[44]
Modified steel slag	aluminum hydroxide	16.40	[63]
Corn stalks	diethylamine	13.60	[64]
Modified cocoa shell	PEI–HCl	86.95	[25]
Modified cocoa shell	APTES-HCl	31.65	**Present study**
Cr(VI)			
Corn stalks	diethylenetriamine	200.00 (303 K)	[23]
Modified granular activated carbon	[3-(methacryloylamino)propyl]-trimethylammonium chloride	81.00	[46]
Spent mushroom (*T. lobayense*)	dodecyl dimethyl benzyl ammonium bromide	43.86	[65]
Sugarcane bagasse	iron(III)-impregnated	13.72	[66]
Brown algae	hydrochloric acid	52.63	[67]
Lagerstroemia speciosa bark	chemical treatment (H_2SO_4/formaldehyde)	24.39	[68]
Giant reed	triethylamine	135	[61]
Lantana camara	sulfuric acid	83.00	[69]
Masau stone	diethylenetriamine	87.32	[37]
Spent substrate (*Auricularia auricular*)	cetyl trimethyl ammonium bromide, immobilized by sodium alginate	27.25	[70]
Macadamia nutshell powder	HCl	44.83	[71]
	NaOH	42.44	
Modified cocoa shell	PEI–HCl	94.34	**[25]**
Modified cocoa shell	APTES-HCl	53.19	**Present study**

3.2.4. Thermodynamic parameters

Thermodynamic parameters such as ΔH°, ΔS° and ΔG° were determined based on Van't Hoff's equations (15-19) to elucidate the adsorption process [72].

$$\theta_e = \frac{q_e}{q_{max}} \quad (15)$$

$$b = \frac{\theta_e}{C_e \times (1-\theta_e)} \quad (16)$$

$$K_{aeq} = \frac{b \times Ma}{\gamma} \quad (17)$$

$$ln(K_{aeq}) = \frac{\Delta S°}{R} - \frac{\Delta H°}{RT} \quad (18)$$

$$\Delta G° = -R \times T \times \ln(K_{aeq}) \quad (19)$$

where θ_e is the fraction of the surface coverage at equilibrium, q_e (mg.g^{-1}) is the amount of ions adsorbed at equilibrium, q_{max} (mg.g^{-1}) is the maximum capacity of the adsorbent, b is the isotherm constant, C_e (mg.L^{-1}) is the equilibrium concentration of ions in solution, K_{aeq} is the equilibrium constant, Ma is the molecular weight of the adsorbent, γ is the activity coefficient, R (8,314 J.K^{-1}.mol^{-1}) is the universal gas constant, and T (K) the absolute temperature. The values of $\Delta G°$, $\Delta H°$ and $\Delta S°$ were obtained from eq.19 and Figure S5, respectively; they are summarized in Table 3. Nitrate and Cr(VI) adsorption presented different behaviors. The negative enthalpy for nitrate proved that the adsorption process was exothermic, indicating that the total energy absorbed in bond breaking was less than the total energy released by adsorbate-adsorbent bond making. Therefore, nitrate adsorption was mainly driven by enthalpy. The negative value of entropy implied a decrease of disorder at the solid-liquid interface associated with a strong interaction at this interface during the adsorption process [73, 74]. Thus, the internal structure of the adsorbent did not seem to be modified during adsorption [72]. Negative values of Gibb's free energy indicated that nitrate adsorption was spontaneous which is in accordance with the fast adsorption process observed in **Figure 3**.

Table 3: Thermodynamic constants for NO_3^- and Cr(VI) adsorption onto ECAB-APTES-HCl (V = 50 mL, m = 0.2 g, 300 rpm).

		$\Delta H°$(kJ.mol^{-1})	$\Delta S°$(J.K^{-1}.mol^{-1})	$\Delta G°$(kJ.mol^{-1})			
	R^2			293 K	303 K	313 K	323 K
NO_3^-	0.993	- 21.57	- 28.41	-13.21	-12.98	-12.78	-12.32
Cr(VI)	0.995	41.70	241.5	- 29.09	-31.36	-34.05	-36.25

For chromium ions, the positive value of enthalpy implied that the adsorption process was endothermic and mainly controlled by physisorption [75]: the ions had to cause more than one water molecule to move. The positive value of entropy indicated some disorder at the liquid/solid interface, suggesting a spontaneous reaction and good affinity of the ions for ECAB-APTES-HCl [76]. $\Delta G°$ was negative, confirming the feasibility and the spontaneity of the adsorption process. Gibb's enthalpy decreased as the temperature increased, so that the diffusion of chromium ions across the external layer boundary and the internal pores was improved when temperature increased [75-77].

4. Desorption of NO_3^- and Cr(VI)

To be useful for industrial applications, the adsorbent should be reusable once saturated with pollutants. Regeneration of the adsorbent should be cheap, effective and harmless to its structure. Sodium hydroxide 0.1 mol/L was a good candidate to remove nitrate and chromium ions [78, 79] from ECAB-APTES-HCl (**Figure 6**). Respective recovery rates of 82% and 79.8% were reached in less than 2 hours. The desorption kinetic confirmed that the adsorption/desorption process was mainly controlled by both physisorption and chemisorption [60, 65]. IR analysis of ECAB-APTES-HCl after desorption studies evidenced a chemical composition of the surface comparable to that of ECAB-APTES-HCl.

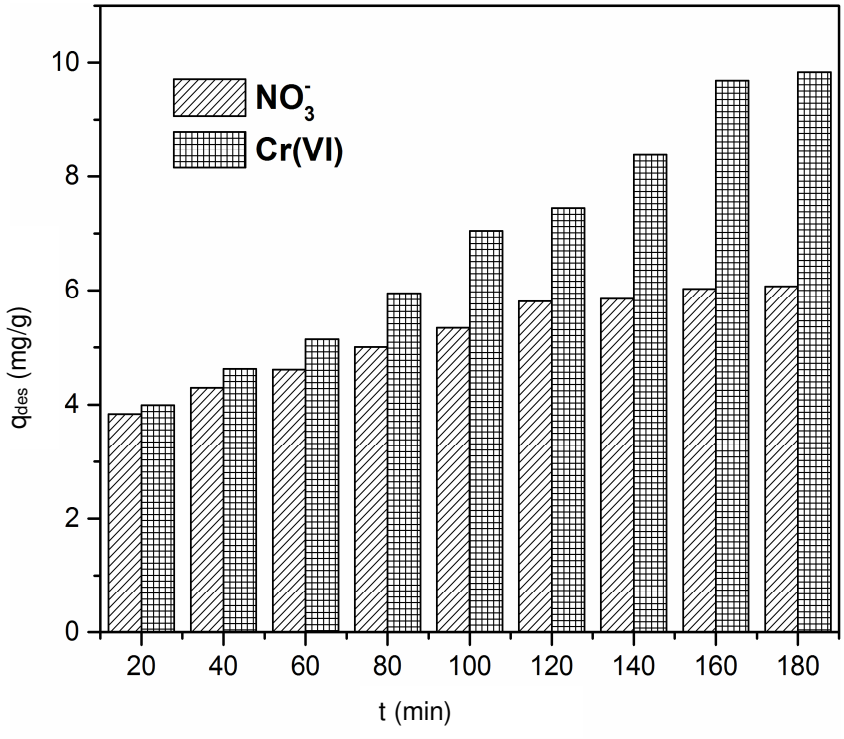

479

480 **Figure 6**: Desorption of NO_3^- and Cr(VI) from ECAB-APTES-HCl (V = 50 mL; m = 0.2 g; 300
481 rpm, pH_i = 5.6 for nitrate and 4.6 for chromate).

482

483 ***5. Proposed adsorption mechanism***

484 The above results show that adsorption is achieved through different steps. Firstly, the pollutants
485 in aqueous solution cover the adsorbent, creating a film layer. Secondly, NO_3^- and Cr(VI) diffuse
486 into the external surface. Thirdly, the pollutants diffuse into the internal adsorption site (**Scheme**
487 **2**). Finally, adsorption occurs on the surface of ECAB-APTES-HCl [49, 80]. As the adsorption
488 process involves both physisorption and chemisorption onto ECAB-APTES-HCl, heavy metal
489 and NO_3^- adsorption can be postulated to take place as follows: (i) an electrostatic interaction
490 occurs between the heavy metal ions (Cr(IV)) and oxygenic functional groups such as hydroxyl
491 and carboxyl functional groups present on ECAB-APTES-HCl; (ii) protonation of the adsorbent
492 introduces NH_3^+ groups, and the surface becomes positively charged. The positively charged

surface slows down/ the interaction with Cr(VI), and NO_3^- adsorption is favored at the adsorbent surface. In addition, the repulsion of Cr(VI) can result in complexation of the solution that reduces chromium ions. In both cases [(i) and (ii)], the pH of the solution plays an important role in the adsorption process: more H^+ ions are available in acidic media, and consequently more NO_3^- is adsorbed, whereas more OH^- ions are available at high pH values and then Cr(VI) is easily adsorbed. This is supported by the kinetic and isotherm studies, pH_{pzc} and ZP measurements. The above results are in agreement with those obtained elsewhere [81].

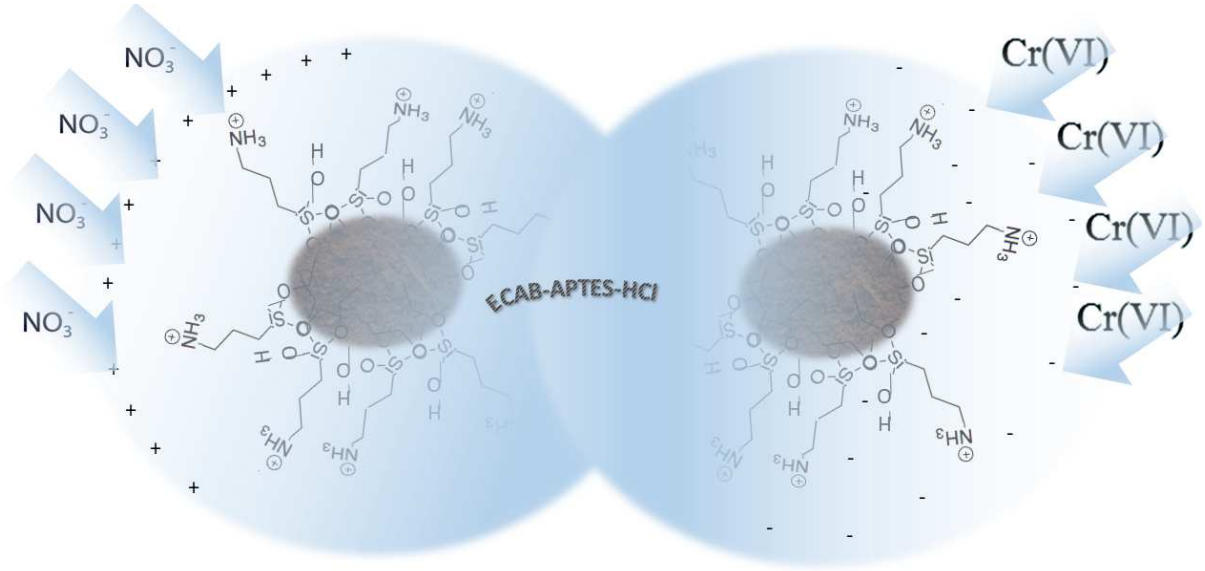

Scheme. 2. Postulated mechanism of nitrate and chromium ion adsorption onto ECAB-APTES-HCl.

Conclusion

Environment-friendly and cost-effective functional cocoa shell (ECAB) was prepared to remove chromium and nitrate pollutants from aqueous solution. Modified ECAB was characterized by FTIR, SEM, EDS, XRD, ZP and DSC, and the successful synthesis and functionalization of ECAB-APTES-HCl was confirmed. Nitrate and chromate are adsorbed onto protonated ECAB-

APTES *via* physical and chemical interactions. Batch mode experiments of nitrate and Cr(VI) adsorption were conducted to determine the kinetic parameters. More than 31 and 53 mg/g of nitrate and Cr(VI) was adsorbed onto the functionalized ECAB-APTES-HCl. These performances were promising in comparison to datas already published with modified vegetal wastes ot biochar. The results fitted well with Langmuir and Freundlich isotherms. Accordingly, functionalized ECAB-APTES-HCl involves physisorption and chemisorption during the adsorption process. The results show that the ECAB-APTES-HCl adsorbent can be used as an efficient and low-cost alternative material to remove chromium and nitrate ions from wastewater.

ACKNOWLEDGMENTS

This work was partially supported by INSA Rouen, Normandy Rouen University, CNRS, Labex SynORg (ANR-11-LABX-0029), the French Embassy in Cameroon (879327A), the Haute Normandie Region (CRUNCH and SéSa networks) and Grand Evreux Agglomération.

REFERENCES

[1] J. Wang, W. Yu, N.J.D. Graham, L. Jiang, Evaluation of a novel polyamide-polyethylenimine nanofiltration membrane for wastewater treatment: Removal of Cu2+ ions, Chemical Engineering Journal, 392 (2020) 123769. https://doi.org/10.1016/j.cej.2019.123769

[2] Y.C. Jordan, A. Ghulam, S. Hartling, Traits of surface water pollution under climate and land use changes: A remote sensing and hydrological modeling approach, Earth-Science Reviews, 128 (2014) 181-195. https://doi.org/10.1016/j.earscirev.2013.11.005

529 [3] S. Lee, E. Lee, J. Ra, B. Lee, S. Kim, S.H. Choi, S.D. Kim, J. Cho, Characterization of marine organic
530 matters and heavy metals with respect to desalination with RO and NF membranes, Desalination, 221
531 (2008) 244-252. https://doi.org/10.1016/j.desal.2007.02.055
532 [4] F. Xu, Z. Liu, Y. Cao, L. Qiu, J. Feng, F. Xu, X. Tian, Assessment of heavy metal contamination in urban
533 river sediments in the Jiaozhou Bay catchment, Qingdao, China, CATENA, 150 (2017) 9-16.
534 https://doi.org/10.1016/j.catena.2016.11.004
535 [5] T.S. Anirudhan, T.A. Rauf, Adsorption performance of amine functionalized cellulose grafted
536 epichlorohydrin for the removal of nitrate from aqueous solutions, J. Ind. Eng. Chem., 19 (2013) 1659-
537 1667. https://doi.org/10.1016/j.jiec.2013.01.036
538 [6] L. Ao, F. Xia, Y. Ren, J. Xu, D. Shi, S. Zhang, L. Gu, Q. He, Enhanced nitrate removal by micro-
539 electrolysis using Fe0 and Surfactant modified activated carbon, Chem. Eng. J., 357 (2018) 180-187.
540 https://doi.org/10.1016/j.cej.2018.09.071
541 [7] I. Aswin Kumar, N. Viswanathan, Development and Reuse of Amine-Grafted Chitosan Hybrid Beads in
542 the Retention of Nitrate and Phosphate, J. Chem. Eng. Data, 63 (2013) 147-158.
543 https://doi.org/10.1021/acs.jced.7b00751
544 [8] J. Elton, K. Hristovski, P. Westerhoff, Titanium Dioxide-Based Hybrid Ion-Exchange Media for
545 Simultaneous Removal of Arsenic and Nitrate, in: Novel Solutions to Water Pollution, American Chemical
546 Society, 2013, pp. 223-236.
547 [9] A. Matilainen, P. Iivari, J. Sallanko, E. Heiska, T. Tuhkanen, The Role of Ozonation and Activated
548 Carbon Filtration in the Natural Organic Matter Removal from Drinking Water, Environ. Technol., 27
549 (2006) 1171-1180. https://doi.org/10.1080/09593332708618731
550 [10] M.Z. Beidokhti, S.T.O. Naeeni, M.S. Abdighahroudi, Biosorption of Nickel (II) from aqueous solutions
551 onto Pistachio Hull waste as a low-cost biosorbent, Civil Engineering Journal, 5 (2019) 447-457.
552 https://doi.org/10.28991/cej-2019-03091259

553 [11] C. Cordier, K. Guyomard, C. Stavrakakis, P. Sauvade, F. Coelho, P. Moulin, Culture of Microalgae with
554 Ultrafiltered Seawater: A Feasibility Study, SciMedicine Journal, 2 (2020) 56-62.
555 https://doi.org/10.28991/SciMedJ-2020-0202-2
556 [12] J. Xu, Z. Cao, Y. Zhang, Z. Yuan, Z. Lou, X. Xu, X. Wang, A review of functionalized carbon nanotubes
557 and graphene for heavy metal adsorption from water: Preparation, application, and mechanism,
558 Chemosphere, 195 (2018) 351-364. https://doi.org/10.1016/j.chemosphere.2017.12.061
559 [13] M. Mahmood-ul-Hassan, M. Yasin, M. Yousra, R. Ahmad, S. Sarwar, Kinetics, isotherms, and
560 thermodynamic studies of lead, chromium, and cadmium bio-adsorption from aqueous solution onto
561 Picea smithiana sawdust, Environmental Science and Pollution Research, 25 (2018) 12570-12578.
562 https://doi.org/10.1007/s11356-018-1300-3
563 [14] J. Bedia, M. Peñas-Garzón, A. Gómez-Avilés, J.J. Rodriguez, C. Belver, 4(4):63., A Review on the
564 Synthesis and Characterization of Biomass-Derived Carbons for Adsorption of Emerging Contaminants
565 from Water, Journal of Carbon Research, 4 (2018) 63. https://doi.org/10.3390/c4040063
566 [15] S. Dogar, S. Nayab, M.Q. Farooq, A. Said, R. Kamran, H. Duran, B. Yameen, Utilization of Biomass Fly
567 Ash for Improving Quality of Organic Dye-Contaminated Water, ACS Omega, 5 (2020) 15850-15864.
568 https://doi.org/10.1021/acsomega.0c00889
569 [16] M.A. Nkansah, M. Donkoh, O. Akoto, J.H. Ephraim, Preliminary studies on the use of sawdust and
570 peanut shell powder as adsorbents for phosphorus removal from water, Emerging Science Journal, 3
571 (2019) 33-40. https://doi.org/10.28991/esj-2019-01166
572 [17] D.L. Ajifack, J.N. Ghogomu, T.D. Noufame, J.N. Ndi, J.M. Ketcha, Adsorption of Cu (II) Ions from
573 Aqueous Solution onto Chemically Prepared Activated Carbon from Theobroma cacoa, Br. J. Appl. Sci.
574 Technol., 4 (2014) 5021-5044. https://doi.org/10.9734/BJAST/2014/12742
575 [18] G.J.F. Cruz, L. Kuboňová, D.Y. Aguirre, L. Matějová, P. Peikertová, I. Troppová, E. Cegmed, A. Wach,
576 P. Kustrowski, M.M. Gomez, L. Obalová, Activated Carbons Prepared from a Broad Range of Residual

577 Agricultural Biomasses Tested for Xylene Abatement in the Gas Phase, ACS Sustainable Chemistry &
578 Engineering, 5 (2017) 2368-2374. https://doi.org/10.1021/acssuschemeng.6b02703
579 [19] S.S. Kalaivani, T. Vidhyadevi, A. Murugesan, P. Baskaralingam, C.D. Anuradha, L. Ravikumar, S.
580 Sivanesan, Equilibrium and kinetic studies on the adsorption of Ni(II) ion from an aqueous solution using
581 activated carbon prepared from Theobroma cacao (cocoa) shell, Desalin. Water Treat., 54 (2015) 1629-
582 1641. https://doi.org/10.1080/19443994.2014.888678
583 [20] N. Bouazizi, J. Vieillard, R. Bargougui, N. Couvrat, O. Thoumire, S. Morin, G. Ladam, N. Mofaddel, N.
584 Brun, A. Azzouz, F. Le Derf, Entrapment and stabilization of iron nanoparticles within APTES modified
585 graphene oxide sheets for catalytic activity improvement, Journal of Alloys and Compounds, 771 (2019)
586 1090-1102. https://doi.org/10.1016/j.jallcom.2018.08.240
587 [21] P.N. Fotsing, E.D. Woumfo, S.A. Măicăneanu, J. Vieillard, C. Tcheka, P.T. Ngueagni, J.M. Siéwé,
588 Removal of Cu(II) from aqueous solution using a composite made from cocoa cortex and sodium
589 alginate, Environmental Science and Pollution Research, 27 (2020) 8451-8466.
590 https://doi.org/10.1007/s11356-019-07206-3
591 [22] J. Vieillard, N. Bouazizi, M.N. Morshed, T. Clamens, F. Desriac, R. Bargougui, P. Thebault, O.
592 Lesouhaitier, F. Le Derf, A. Azzouz, CuO Nanosheets Modified with Amine and Thiol Grafting for High
593 Catalytic and Antibacterial Activities, Industrial & Engineering Chemistry Research, 58 (2019) 10179-
594 10189. https://doi.org/10.1021/acs.iecr.9b00609
595 [23] Chen, Q. Yue, B. Gao, Q. Li, X. Xu, Removal of Cr(VI) from aqueous solution using modified corn
596 stalks: Characteristic, equilibrium, kinetic and thermodynamic study, Chem. Eng. J., 168 (2011) 909-917.
597 https://doi.org/10.1016/j.cej.2011.01.063
598 [24] Y. Li, X. Lin, X. Zhuo, X. Luo, Poly(vinyl alcohol)/quaternized lignin composite absorbent: Synthesis,
599 characterization and application for nitrate adsorption, Journal of Applied Polymer Science, 128 (2013)
600 2746-2752. 10.1002/app.38437

601 [25] P.N. Fotsing, E.D. Woumfo, S. Mezghich, M. Mignot, N. Mofaddel, F. Le Derf, J. Vieillard, Surface
602 modification of biomaterials based on cocoa shell with improved nitrate and Cr(vi) removal, RSC
603 Advances, 10 (2020) 20009-20019. https://doi.org/10.1039/D0RA03027A
604 [26] R. Bargougui, N. Bouazizi, N. Brun, P.N. Fotsing, O. Thoumire, G. Ladam, E.D. Woumfo, N. Mofaddel,
605 F.L. Derf, J. Vieillard, Improvement in CO_2 adsorption capacity of cocoa shell through functionalization
606 with amino groups and immobilization of cobalt nanoparticles, J. Environ. Chem. Eng., 6 (2018) 325-331.
607 https://doi.org/10.1016/j.jece.2017.11.079
608 [27] Q. Qin, J. Ma, K. Liu, Adsorption of anionic dyes on ammonium-functionalized MCM-41, J. Hazard.
609 Mater., 162 (2009) 133-139. https://doi.org/10.1016/j.jhazmat.2008.05.016
610 [28] L.D. Hafshejani, S.B. Nasab, R.M. Gholami, M. Moradzadeh, Z. Izadpanah, S.B. Hafshejani, A.
611 Bhatnagar, Removal of zinc and lead from aqueous solution by nanostructured cedar leaf ash as
612 biosorbent, J. Mol. Liq., 211 (2015) 448-456. https://doi.org/10.1016/j.molliq.2015.07.044
613 [29] J. Maity, S.K. Ray, Enhanced adsorption of Cr(VI) from water by guar gum based composite
614 hydrogels, Int. J. Biol. Macromol., 89 (2016) 246-255. https://doi.org/10.1016/j.ijbiomac.2016.04.036
615 [30] A.M.E. Khalil, O. Eljamal, T.W.M. Amen, Y. Sugihara, N. Matsunaga, Optimized nano-scale zero-
616 valent iron supported on treated activated carbon for enhanced nitrate and phosphate removal from
617 water, Chem. Eng. J., 309 (2017) 349-365. https://doi.org/10.1016/j.cej.2016.10.080
618 [31] J.M. Siéwé, E. Djoufac Woumfo, P. Djomgoue, D. Njopwouo, Activation of clay surface sites of
619 Bambouto's Andosol (Cameroon) with phosphate ions: Application for copper fixation in aqueous
620 solution, Appl. Clay Sci., 114 (2015) 31-39. https://doi.org/10.1016/j.clay.2015.05.003
621 [32] R. Redgwell, V. Trovato, S. Merinat, D. Curti, S. Hediger, A. Manez, Dietary fibre in cocoa shell:
622 characterisation of component polysaccharides, Food Chemistry, 81 (2003) 103-112.
623 https://doi.org/10.1016/S0308-8146(02)00385-0

624 [33] N. Majoul, S. Aouida, B. Bessaïs, Progress of porous silicon APTES-functionalization by FTIR
625 investigations, Applied Surface Science, 331 (2015) 388-391.
626 https://doi.org/10.1016/j.apsusc.2015.01.107
627 [34] F.l. Pua, M.S. Sajab, C.H. Chia, S. Zakaria, I.A. Rahman, M.S. Salit, Alkaline-treated cocoa pod husk as
628 adsorbent for removing methylene blue from aqueous solutions, Journal of Environmental Chemical
629 Engineering, 1 (2013) 460-465. https://doi.org/10.1016/j.jece.2013.06.012
630 [35] V. Hospodarova, E. Singovszka, N. Stevulova, Characterization of Cellulosic Fibers by FTIR
631 Spectroscopy for Their Further Implementation to Building Materials, American Journal of Analytical
632 Chemistry, 9 (2018) 303-310. https://doi.org/10.4236/ajac.2018.96023
633 [36] M.N. Sepehr, H. Kazemian, E. Ghahramani, A. Amrane, V. Sivasankar, M. Zarrabi, Defluoridation of
634 water via Light Weight Expanded Clay Aggregate (LECA): Adsorbent characterization, competing ions,
635 chemical regeneration, equilibrium and kinetic modeling, J. Taiwan Inst. Chem. Eng., 45 (2014) 1821-
636 1834. https://doi.org/10.1016/j.jtice.2014.02.009
637 [37] A.B. Albadarin, S. Solomon, T.A. Kurniawan, C. Mangwandi, G. Walker, Single, simultaneous and
638 consecutive biosorption of Cr(VI) and Orange II onto chemically modified masau stones, J. Environ.
639 Manage., 204 (2017) 365-374. https://doi.org/10.1016/j.jenvman.2017.08.042
640 [38] D.D. Asouhidou, K.S. Triantafyllidis, N.K. Lazaridis, K.A. Matis, Adsorption of Remazol Red 3BS from
641 aqueous solutions using APTES- and cyclodextrin-modified HMS-type mesoporous silicas, Colloids Surf.,
642 A, 346 (2009) 83-90. https://doi.org/10.1016/j.colsurfa.2009.05.029
643 [39] R. Kishor, A.K. Ghoshal, APTES grafted ordered mesoporous silica KIT-6 for CO_2 adsorption, Chem.
644 Eng. J., 262 (2015) 882-890. https://doi.org/10.1016/j.cej.2014.10.039
645 [40] W.-H. Chen, P.-C. Kuo, Isothermal torrefaction kinetics of hemicellulose, cellulose, lignin and xylan
646 using thermogravimetric analysis, Energy, 36 (2011) 6451-6460.
647 https://doi.org/10.1016/j.energy.2011.09.022

[41] A. Moubarik, N. Grimi, Valorization of olive stone and sugar cane bagasse by-products as biosorbents for the removal of cadmium from aqueous solution, Food Res. Int., 73 (2015) 169-175. https://doi.org/10.1016/j.foodres.2014.07.050

[42] T. Wu, G. Wang, F. Zhan, Q. Dong, Q. Ren, J. Wang, J. Qiu, Surface-treated carbon electrodes with modified potential of zero charge for capacitive deionization, Water Res., 93 (2016) 30-37. https://doi.org/10.1016/j.watres.2016.02.004

[43] Q.-Q. Zhong, Q.-Y. Yue, Q. Li, B.-Y. Gao, X. Xu, Removal of Cu(II) and Cr(VI) from wastewater by an amphoteric sorbent based on cellulose-rich biomass, Carbohydr. Polym., 111 (2014) 788-796. https://doi.org/10.1016/j.carbpol.2014.05.043

[44] A. Rajeswari, A. Amalraj, A. Pius, Adsorption studies for the removal of nitrate using chitosan/PEG and chitosan/PVA polymer composites, J. Water Process. Eng., 9 (2016) 123-134. https://doi.org/10.1016/j.jwpe.2015.12.002

[45] S. Rangabhashiyam, P. Balasubramanian, Adsorption behaviors of hazardous methylene blue and hexavalent chromium on novel materials derived from Pterospermum acerifolium shells, J. Mol. Liq., 254 (2018) 433-445. https://doi.org/10.1016/j.molliq.2018.01.131

[46] D.-W. Cho, C.-M. Chon, Y. Kim, B.-H. Jeon, F.W. Schwartz, E.-S. Lee, H. Song, Adsorption of nitrate and Cr(VI) by cationic polymer-modified granular activated carbon, Chem. Eng. J., 175 (2011) 298-305. https://doi.org/10.1016/j.cej.2011.09.108

[47] R. Saad, K. Belkacemi, S. Hamoudi, Adsorption of phosphate and nitrate anions on ammonium-functionalized MCM-48: Effects of experimental conditions, J. Colloid Interface Sci., 311 (2007) 375-381. https://doi.org/10.1016/j.jcis.2007.03.025

[48] T. Chen, Z. Zhou, S. Xu, H. Wang, W. Lu, Adsorption behavior comparison of trivalent and hexavalent chromium on biochar derived from municipal sludge, Bioresource Technology, 190 (2015) 388-394. https://doi.org/10.1016/j.biortech.2015.04.115

672 [49] W.N. Nyairo, Y.R. Eker, C. Kowenje, E. Zor, H. Bingol, A. Tor, D.M. Ongeri, Efficient Removal of
673 Lead(II) Ions from Aqueous Solutions Using Methyl-β-Cyclodextrin Modified Graphene Oxide, Water, Air,
674 & Soil Pollution, 228 (2017) 406. https://doi.org/10.1007/s11270-017-3589-9
675 [50] R.-Z. Wang, D.-L. Huang, Y.-G. Liu, C. Zhang, C. Lai, G.-M. Zeng, M. Cheng, X.-M. Gong, J. Wan, H. Luo,
676 Investigating the adsorption behavior and the relative distribution of Cd2+ sorption mechanisms on
677 biochars by different feedstock, Bioresource Technology, 261 (2018) 265-271.
678 https://doi.org/10.1016/j.biortech.2018.04.032
679 [51] S. Mohan, V. Kumar, D.K. Singh, S.H. Hasan, Effective removal of lead ions using graphene oxide-
680 MgO nanohybrid from aqueous solution: Isotherm, kinetic and thermodynamic modeling of adsorption,
681 Journal of Environmental Chemical Engineering, 5 (2017) 2259-2273.
682 https://doi.org/10.1016/j.jece.2017.03.031
683 [52] Q. Zhou, Y. Duan, C. Zhu, J. Zhang, M. She, H. Wei, Y. Hong, Adsorption equilibrium, kinetics and
684 mechanism studies of mercury on coal-fired fly ash, Korean Journal of Chemical Engineering, 32 (2015)
685 1405-1413. https://doi.org/10.1007/s11814-014-0336-4
686 [53] F.M. Machado, C.P. Bergmann, E.C. Lima, B. Royer, F.E. de Souza, I.M. Jauris, T. Calvete, S.B. Fagan,
687 Adsorption of Reactive Blue 4 dye from water solutions by carbon nanotubes: experiment and theory,
688 Phys. Chem. Chem. Phys., 14 (2012) 11139-11153. https://doi.org/10.1039/C2CP41475A
689 [54] T. Jóźwiak, U. Filipkowska, P. Szymczyk, A. Mielcarek, Sorption of nutrients (orthophosphate, nitrate
690 III and V) in an equimolar mixture of P–PO_4, N–NO_2 and N–NO_3 using chitosan, Arabian J. Chem., 12
691 (2016) 4104-4117. https://doi.org/10.1016/j.arabjc.2016.04.008
692 [55] Y.W. Berkessa, S.T. Mereta, F.F. Feyisa, Simultaneous removal of nitrate and phosphate from
693 wastewater using solid waste from factory, Appl. Water Sci., 9 (2019) 28.
694 https://doi.org/10.1007/s13201-019-0906-z

695 [56] M.A. Fulazzaky, Z. Majidnia, A. Idris, Mass transfer kinetics of Cd(II) ions adsorption by titania
696 polyvinylalcohol-alginate beads from aqueous solution, Chemical Engineering Journal, 308 (2017) 700-
697 709. https://doi.org/10.1016/j.cej.2016.09.106
698 [57] M.A. Al-Ghouti, J. Li, Y. Salamh, N. Al-Laqtah, G. Walker, M.N.M. Ahmad, Adsorption mechanisms of
699 removing heavy metals and dyes from aqueous solution using date pits solid adsorbent, J. Hazard.
700 Mater., 176 (2010) 510-520. https://doi.org/10.1016/j.jhazmat.2009.11.059
701 [58] C.S.T. Araújo, I.L.S. Almeida, H.C. Rezende, S.M.L.O. Marcionilio, J.J.L. Léon, T.N. de Matos,
702 Elucidation of mechanism involved in adsorption of Pb(II) onto lobeira fruit (Solanum lycocarpum) using
703 Langmuir, Freundlich and Temkin isotherms, Microchem. J., 137 (2018) 348-354.
704 https://doi.org/10.1016/j.microc.2017.11.009
705 [59] E. Inam, U.J. Etim, E.G. Akpabio, S.A. Umoren, Process optimization for the application of carbon
706 from plantain peels in dye abstraction, J. Taibah Univ. Sci., 11 (2017) 173-185.
707 https://doi.org/10.1016/j.jtusci.2016.01.003
708 [60] A.A. Inyinbor, F.A. Adekola, G.A. Olatunji, Kinetics, isotherms and thermodynamic modeling of liquid
709 phase adsorption of Rhodamine B dye onto Raphia hookerie fruit epicarp, Water Resour. Ind., 15 (2016)
710 14-27. https://doi.org/10.1016/j.wri.2016.06.001
711 [61] Z. Ren, X. Xu, X. Wang, B. Gao, Q.-Y. Yue, W. Song, L. Zhang, H. Wang, FTIR, Raman, and XPS analysis
712 during phosphate, nitrate and Cr(VI) removal by amine cross-linking biosorbent, J. Colloid Interface Sci.,
713 468 (2016) 313-323. https://doi.org/10.1016/j.jcis.2016.01.079
714 [62] H. Song, Z. Yao, C. Shuang, A. Li, Accelerated removal of nitrate from aqueous solution by utilizing
715 polyacrylic anion exchange resin with magnetic separation performance, J. Ind. Eng. Chem., 20 (2014)
716 2888-2894. https://doi.org/10.1016/j.jiec.2013.11.024
717 [63] L. Yang, M. Yang, P. Xu, X. Zhao, H. Bai, H. Li, Characteristics of Nitrate Removal from Aqueous
718 Solution by Modified Steel Slag, Water, 9 (2017) 757. https://doi.org/10.3390/w9100757

719 [64] C. Fan, X. Wang, B. Xu, Y. Wang, D. Liu, M. Zhang, Y. Shang, F. Dai, L. Zhang, D. Sun, Amino-
720 functionalized MOFs with high physicochemical stability for efficient gas storage/separation, dye
721 adsorption and catalytic performance, J. Mater. Chem. A, 6 (2018) 24486-24495.
722 https://doi.org/10.1039/C8TA07839D
723 [65] X. Jing, Y. Cao, X. Zhang, D. Wang, X. Wu, H. Xu, Biosorption of Cr(VI) from simulated wastewater
724 using a cationic surfactant modified spent mushroom, Desalination, 269 (2011) 120-127.
725 https://doi.org/10.1016/j.desal.2010.10.050
726 [66] Y. Zhu, H. Zhang, H. Zeng, M. Liang, R. Lu, Adsorption of chromium (VI) from aqueous solution by the
727 iron (III)-impregnated sorbent prepared from sugarcane bagasse, Int. J. Environ. Sci. Technol., 9 (2012)
728 463-472. https://doi.org/10.1007/s13762-012-0043-9
729 [67] T. Ainane, A. Abourriche, M. Kabbaj, M. Elkouali, A. Bennamara, M. Charrouf, M. Talbi, Removal of
730 hexavalent chromium from aqueous solution by raw and chemically modified seaweed Bifurcaria
731 bifurcata, J. Mater. Environ. Sci., 5 (2014) 975-982.
732 [68] S. Srivastava, S.B. Agrawal, M.K. Mondal, Biosorption isotherms and kinetics on removal of Cr(VI)
733 using native and chemically modified Lagerstroemia speciosa bark, Ecol. Eng., 85 (2015) 56-66.
734 https://doi.org/10.1016/j.ecoleng.2015.10.011
735 [69] K. Nithya, A. Sathish, P. Senthil Kumar, T. Ramachandran, Biosorption of hexavalent chromium from
736 aqueous solution using raw and acid-treated biosorbent prepared from Lantana camara fruit, Desalin.
737 Water Treat., 57 (2016) 25097-25113. https://doi.org/10.1080/19443994.2016.1145605
738 [70] T. Zang, Z. Cheng, L. Lu, Y. Jin, X. Xu, W. Ding, J. Qu, Removal of Cr(VI) by modified and immobilized
739 Auricularia auricula spent substrate in a fixed-bed column, Ecol. Eng., 99 (2017) 358-365.
740 https://doi.org/10.1016/j.ecoleng.2016.11.070

741 [71] V.E. Pakade, T.D. Ntuli, A.E. Ofomaja, Biosorption of hexavalent chromium from aqueous solutions
742 by Macadamia nutshell powder, Appl. Water Sci., 7 (2017) 3015-3030. https://doi.org/10.1007/s13201-
743 016-0412-5
744 [72] P.S. Ghosal, A.K. Gupta, Determination of thermodynamic parameters from Langmuir isotherm
745 constant-revisited, Journal of Molecular Liquids, 225 (2017) 137-146.
746 https://doi.org/10.1016/j.molliq.2016.11.058
747 [73] C. Fan, Y. Zhang, Adsorption isotherms, kinetics and thermodynamics of nitrate and phosphate in
748 binary systems on a novel adsorbent derived from corn stalks, J. Geochem. Explor., 188 (2018) 95-100.
749 https://doi.org/10.1016/j.gexplo.2018.01.020
750 [74] H. Koyuncu, A.R. Kul, A. Çalımlı, N. Yıldız, H. Ceylan, Adsorption of dark compounds with bentonites
751 in apple juice, LWT--Food Sci. Technol., 40 (2007) 489-497. https://doi.org/10.1016/j.lwt.2005.12.005
752 [75] S. Mylsamy, C. Theivarasu, Adsorption of Reactive Dye Using Low Cost Adsorbent: Cocoa
753 (Theobroma Cacao) Shell, World J. Appl. Chem. Environ. Chem., 1 (2012) 22-29.
754 [76] O.S. Bello, M.A. Ahmad, T.T. Siang, Utilization of Cocoa Pod Husk for the Removal of Remazol Black B
755 Reactive Dye from Aqueous Solutions: Kinetic, Equilibrium and Thermodynamic Studies, Trends Appl. Sci.
756 Res., 6 (2011) 794-812. https://doi.org/10.3923/tasr.2011.794.812
757 [77] S. B., J. Zhang, H. Wang, H. Yin, H. Chen, The influence of pH, co-existing ions, ionic strength, and
758 temperature on the adsorption and reduction of hexavalent chromium by undissolved humic acid,
759 Chemosphere, 212 (2018) 209-218. https://doi.org/10.1016/j.chemosphere.2018.08.067
760 [78] V.K. Gupta, A. Rastogi, Biosorption of hexavalent chromium by raw and acid-treated green alga
761 Oedogonium hatei from aqueous solutions, J. Hazard. Mater., 163 (2009) 396-402.
762 https://doi.org/10.1016/j.jhazmat.2008.06.104

763 [79] U.S. Orlando, A.U. Baes, W. Nishijima, M. Okada, Preparation of agricultural residue anion
764 exchangers and its nitrate maximum adsorption capacity, Chemosphere, 48 (2002) 1041-1046.
765 https://doi.org/10.1016/S0045-6535(02)00147-9
766 [80] L. Largitte, R. Pasquier, A review of the kinetics adsorption models and their application to the
767 adsorption of lead by an activated carbon, Chemical Engineering Research and Design, 109 (2016) 495-
768 504. https://doi.org/10.1016/j.cherd.2016.02.006
769 [81] D. Guo, R. Shibuya, C. Akiba, S. Saji, T. Kondo, J. Nakamura, Active sites of nitrogen-doped carbon
770 materials for oxygen reduction reaction clarified using model catalysts, Science, 351 (2016) 361.
771 https://doi.org/10.1126/science.aad0832

772

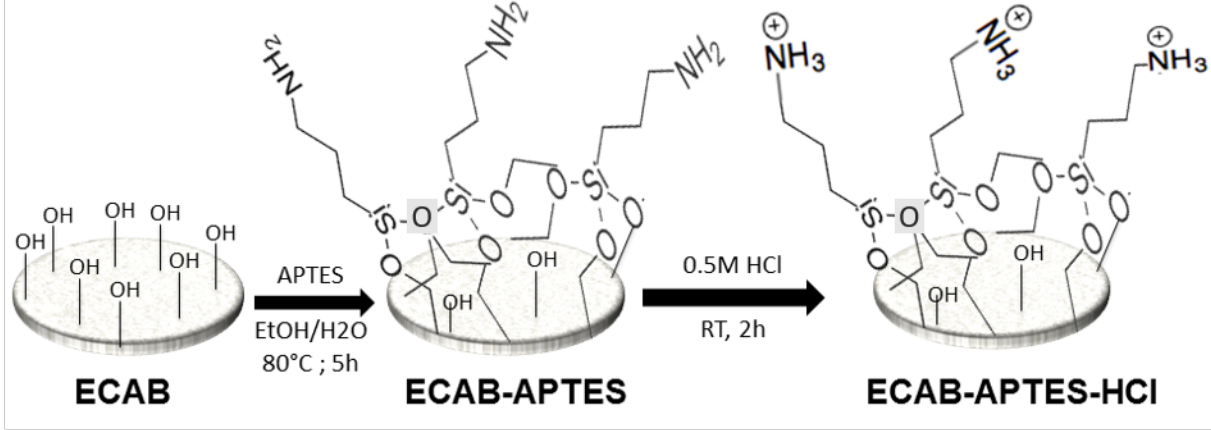
OH
APTES
EtOH/H2O
80°C ; 5h
NH2
0.5M HCl
RT, 2h
NH3
ECAB
ECAB-APTES
ECAB-APTES-HCl